

Synergistic effect of mesoporous Mn_2O_3 -supported Pd nanoparticle catalysts for electrocatalytic oxygen reduction reaction with enhanced performance in alkaline medium†

Cite this: *J. Mater. Chem. A*, 2014, 2, 1272

Received 7th September 2013
Accepted 12th November 2013

DOI: 10.1039/c3ta13585c

www.rsc.org/MaterialsA

Hui-Qing Dong, Yu-Yun Chen, Min Han, Shun-Li Li, Jie Zhang, Ji-Sen Li, Ya-Qian Lan,* Zhi-Hui Dai and Jian-Chun Bao*

We synthesized a novel mesoporous Mn_2O_3 nanostructure as an electrocatalyst support, then Pd- Mn_2O_3 with different Pd loading amounts were obtained by a facile solvothermal method. The Pd- Mn_2O_3 demonstrated a good competitive ORR activity and a high selectivity in alkaline medium, which can be comparable to commercial Pt/C catalysts.

The fuel cell is an important energy conversion device to solve the currently faced issue concerning the environment and energy. One of the technical challenges in fuel cells is the sluggish kinetics of the oxygen reduction reaction (ORR) at the cathode,^{1,2} so developing efficient catalysts for negative electrode ORR plays a significant role in various energy storage and conversion technologies. Currently, metals and their alloys are commonly the catalysts for ORR.^{3,4} However, metal catalysts frequently suffer from dissolution, sintering and agglomeration during fuel cell operation which can reduce activity and durability.⁵ An effective strategy is the use of a proper support to enhance the stability and dispersity of the metal.⁶ The carbon materials,^{7,8} mesoporous silicon⁹ and transition metal oxides^{10,11} have been used as electrocatalyst supports for ORR in previous studies. The transition metal oxides are considered to be attractive candidates as solid support for nanocatalytic systems because of their high thermal, mechanical and oxidative stability and strong interaction with the metal.^{12,13} In addition, mesoporous materials are also widely used as electrocatalyst support due to their large specific surface area and unique pore structure which can permit more active sites for the contact between catalysts and electrolytes.^{14,15} So it is a significant and challengeable task to synthesize metal nanoparticles loaded mesoporous transition metal oxides as ORR electrocatalysts, which may kill two birds with one stone. Firstly, the

strong interaction between metal and mesoporous transition metal oxide can enhance the stability of the metal,¹⁶ and the mesoporous structure can also facilitate the diffusion, adsorption and transport of O_2 during the process of ORR.¹⁷ Furthermore, the synergetic effects of support with metal occasionally may lead to improved catalytic performance, which cannot be achieved by using a single catalyst.¹⁸ So far, catalysts of metal nanoparticles loaded mesoporous metal oxides have not been reported.

Among the various candidates for non-Pt metal catalysts, Pd has been researched extensively as an ORR catalyst due to its relatively higher activity.^{19,20} Also, manganese oxides, with the advantages of low cost, high elemental abundance and minimum environmental impact, are widely used as catalysts in diverse areas.^{21,22} Particularly, some MnO_x phases have been shown to have good electrocatalytic activity for ORR in alkaline fuel cells.^{23–25} Therefore, these inspire us to employ mesoporous manganese oxides supporting Pd nanoparticles as electrocatalysts for ORR.

Here, we report a novel Mn_2O_3 support with unique mesoporous structure, which exhibits an excellent ORR activity. Firstly we obtained various Pd loading amounts (10%, 20% and 30%) of Pd- Mn_2O_3 nanocomposites by a facile solvothermal method. The composites of Pd- Mn_2O_3 demonstrated a good competitive ORR activity and a high selectivity, which can be comparable to commercial Pt/C catalysts in 0.1 M KOH solution. The Pd- Mn_2O_3 nanocomposites exhibited a higher catalytic stability than Pt/C in alkaline electrolyte. We think that their excellent catalytic performance originates from not only the synergetic effects between the Pd nanoparticles and Mn_2O_3 , but also the characteristic of mesoporous architecture.

The synthesis of mesoporous Mn_2O_3 nanostructure was performed by modifying a microemulsion method between $\text{Mn}(\text{Ac})_2$ and Na_3PO_4 in alkaline media. Tetrabutyl ammonium hydroxide aqueous solution (10%) was employed to adjust the pH value of the reaction solution. The Pd- Mn_2O_3 nanocomposites with different Pd loading amounts were achieved by simple solvothermal method as described in the ESI.† Several

Jiangsu Key Laboratory of Biomedical Materials, College of Chemistry and Materials Science, Nanjing Normal University, Nanjing 210023, People's Republic of China. E-mail: yqlan@njnu.edu.cn; baojianchun@njnu.edu.cn

† Electronic supplementary information (ESI) available: Experimental details and additional figures as noted in the text. See DOI: 10.1039/c3ta13585c

obvious and sharp diffraction peaks can be observed from the powder X-ray diffraction (XRD) patterns (Fig. 1a). The result shows that the products obtained are well crystallized. Compared with the standard cards (JCPD-87-639 for cubic Pd and JCPDS-76-150 for cubic Mn_2O_3), no shift of Pd and Mn_2O_3 peaks indicates that the products obtained are Pd- Mn_2O_3 nanocomposites rather than Pd-Mn alloy. The actual Pd loading amounts of the different Pd- Mn_2O_3 nanocomposites by the inductively coupled plasma (ICP) were about 9.36, 20.87 and 31.62%, respectively, which are close to the initial designed loading amounts (10, 20 and 30 wt%). The transmission electron microscope (TEM) image shows that many tiny particles assembled onto the mesoporous nanostructure (Fig. 1b). The lattice fringes are about 0.27 nm (Fig. 1d), which match the (222) facet of Mn_2O_3 very well. Pd particles (about 20 nm) are synthesized and well dispersed onto the Mn_2O_3 support (Fig. 1c). For the Pd nanoparticles section (Fig. 1e), clear lattice fringes (0.22 nm) are observed, corresponding to the (111) plane of cubic phase Pd. Energy dispersive spectrometer (EDS) analyses show the main elements in the obtained samples (Fig. S1†).

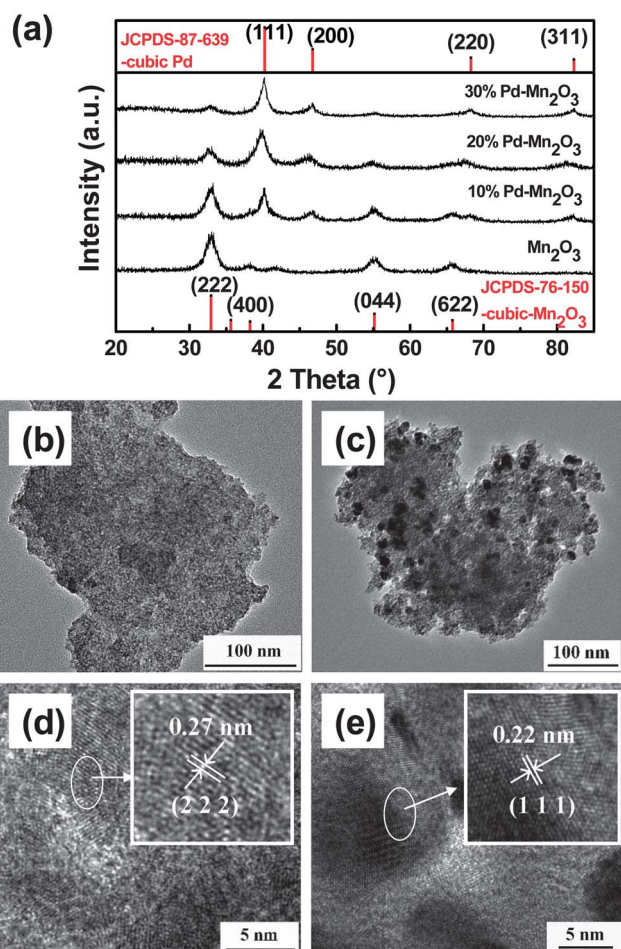


Fig. 1 (a) XRD patterns of mesoporous Mn_2O_3 nanostructure and Pd- Mn_2O_3 nanocomposites with different Pd loading amounts. TEM images of (b) mesoporous Mn_2O_3 nanostructure (c) 10% Pd- Mn_2O_3 nanocomposite and HRTEM images of (d) mesoporous Mn_2O_3 nanostructure (e) 10% Pd- Mn_2O_3 nanocomposite.

The detected C element originates from the surface capping reagent or absorbed air. And the detected P element is from Na_3PO_4 .

The composition and oxidation state of obtained samples are also confirmed by X-ray Photoelectron Spectroscopy (XPS) (Fig. S2†). The spin-orbit splitting is observed in Mn 2p, which is the difference between binding energy values of the Mn $2p_{3/2}$ and Mn $2p_{1/2}$ levels. Similar to Mn_2O_3 reported in the literature,²⁶ the observed spin-orbit splitting is 11.7 eV. Similar spin-orbit splitting values are also observed in the nanocomposites (Fig. 2a). The core-level Pd 3d spectrum of Pd- Mn_2O_3 nanocomposites displays a doublet signal (Fig. 2b). Pd peaks are assigned to Pd at 335.1 and 340.2 eV for Pd $3d_{5/2}$ and Pd $3d_{3/2}$, respectively. Other weak peaks at 336.2, 337.3, and 342.2 eV can be assigned to PdO and PdO₂. Compared with 335.1 eV for pure Pd $3d_{5/2}$,²⁷ the peak shift is not observed in the Pd 3d XPS. This result means the dominant phases of the obtained composites are metallic Pd and Mn_2O_3 , and this corresponds to the XRD result.

To prove the effect of Na_3PO_4 in the reaction system, we performed other condition experiments, where the morphology and composition of products had a great difference, by adding different amounts of Na_3PO_4 . If no Na_3PO_4 was added, Mn_3O_4 nanospheres with a particle size of 13 nm can be obtained (Fig. S3a and S4a†). While the mixed phase of Mn_2O_3 and Mn_3O_4 was obtained when the amount of Na_3PO_4 was 1 M (Fig. S3b and S4b†). So the amount of Na_3PO_4 has a great influence on the formation of mesoporous Mn_2O_3 nanostructure.

The nitrogen adsorption-desorption isotherms of Mn_2O_3 nanostructure and Pd- Mn_2O_3 nanocomposites are type-IV with a distinct hysteresis loop (Fig. 3a and S5†). The pore size distribution curves of Mn_2O_3 and Pd- Mn_2O_3 nanocomposites are in the range from 3–5 nm (Fig. 3b). Both the results suggest that the Mn_2O_3 support and nanocomposites have the mesoporous architecture. The Brunauer-Emmett-Teller (BET) surface area and the pore size of Mn_2O_3 nanostructure were measured to be $246 \text{ m}^2 \text{ g}^{-1}$ and 3.7 nm, respectively. With the increase of Pd loading, the surface area of Pd- Mn_2O_3

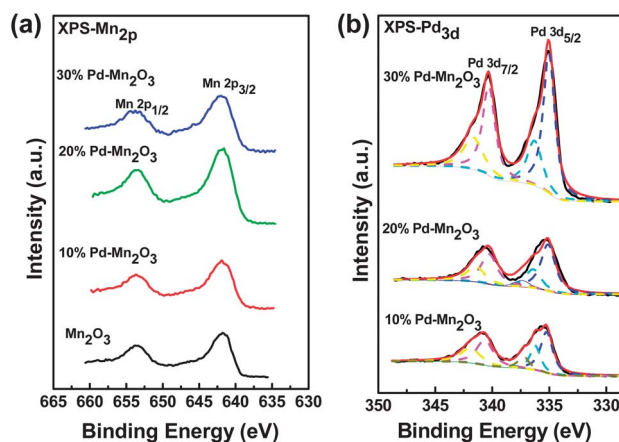


Fig. 2 XPS spectra of (a) Mn 2p and (b) Pd 3d of the prepared samples.

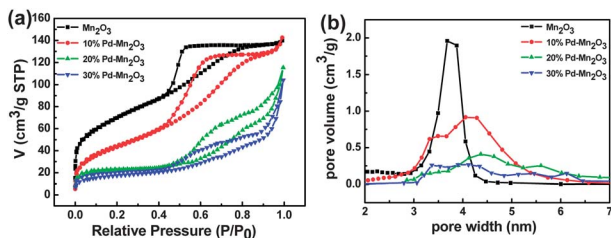


Fig. 3 (a) N_2 adsorption-desorption isotherms and (b) their corresponding pore size distributions of mesoporous Mn_2O_3 nanostructure and Pd- Mn_2O_3 nanocomposites with different Pd loading amounts.

nanocomposites decreased, while the pore size displayed no significant variation (Table S1[†]). This mesoporous structure can provide the possibility of efficient mass transport and thus lead to enhanced electrocatalytic performance.

The electrocatalytic activity of the prepared catalysts for ORR was characterized by cyclic voltammetry (CV) in 0.1 M KOH on a glassy carbon electrode. CV curves of the catalysts are shown at a scan rate of 50 mV s⁻¹ in O_2 -saturated and N_2 -saturated 0.1 M KOH solutions (Fig S6[†]). Compared with the featureless reduction current in N_2 -saturated electrolyte, the detected current under O_2 atmosphere was attributed to the catalytic oxygen reduction. Rotating-disk electrode (RDE) measurements were further carried out to reveal the ORR kinetics of these obtained catalysts. Fig. S7[†] shows the linear sweeping voltammogram (LSVs) of Mn_2O_3 and Pd- Mn_2O_3 at different electrode rotating rates. The increase in current with faster rotating rates is expected, as faster rotating rates correlate with faster O_2 flux to the catalyst surface. The LSVs show that the ORR onset potential of mesoporous Mn_2O_3 is -0.11 V and Pd- Mn_2O_3 with Pd loading amounts of 10%, 20% and 30% are 0, 0.02 and 0.03 V at 1600 rpm vs. the saturated calomel electrode (SCE), respectively (Fig. 4a). The nanocomposites after loading Pd

nanoparticles show more positive onset potential than mesoporous Mn_2O_3 . This result reveals that the synergetic cocatalytic effect between the Pd nanoparticles and Mn_2O_3 support is favorable to enhance the catalytic activity.

The four-electron reduction of O_2 to H_2O has attracted a lot of attention in view of its important application in fuel cells. The electron transfer number n can be determined from the slope of the fitted linear Koutecky-Levich (K-L) plot (j^{-1} vs. $\omega^{-1/2}$) lines. The slope of the linear K-L line for the mesoporous Mn_2O_3 is obviously higher than that of Pd- Mn_2O_3 (Fig. 4b), indicating a lower transferred electron number. Fig. S8[†] shows the electron transfer number of synthesized catalysts at various potentials, in which mesoporous Mn_2O_3 mainly proceeded through a two-electron (2e) reduction while Pd- Mn_2O_3 nanocomposites catalyzed the oxygen reduction *via* a quasi-4e pathway. The high electron transfer number further confirms the high ORR efficiency of the Pd- Mn_2O_3 nanocomposite catalysts.

To further illustrate the high ORR catalysis activity of Pd- Mn_2O_3 , the LSVs of obtained nanocomposites, commercial 10% Pd/C, commercial 20% Pt/C and Pd/graphene have been considered at 1600 rpm (Fig. 4d). The level of the catalytic activity can be found from Table S2[†]. Compared with Pd/graphene, 10% Pd- Mn_2O_3 shows a large positive shift in onset potential (*ca.* 0.1 V) and similar current density. For commercial 10% Pd/C and 10% Pd- Mn_2O_3 , the 10% Pd- Mn_2O_3 exhibits higher onset potential and lower current density. These results suggest that the mesoporous architecture of Mn_2O_3 support with high BET surface area can maybe enhance the catalytic performance. The LSV of 20% Pd- Mn_2O_3 shows a positive onset potential and a current density of 2.31 mA cm⁻². The onset potential is similar to that of commercial 20% Pt/C. Increasing the Pd loading amount to 30%, the Pd- Mn_2O_3 has no significant increase in onset potential and a slight increase of current density. The results may illustrate that the catalytic activity not only depends on the loading amount of metal, but also closely relates to the pore structure of the support. Therefore, the prepared 20% Pd- Mn_2O_3 catalyst is found to be an efficient replaceable electrocatalyst for the ORR.

Fig 4c displays the Tafel plots of nanocomposites in alkaline electrolyte. Kinetic currents (i_k) derived from the mass-transport correction ($i_k = (i \times i_d)/(i_d - i)$) are employed to construct the Tafel curves (i is the measured current density, i_d is the diffusion-limiting current density). It is worth reminding that the higher the Tafel slope is, the faster the overpotential increase with the current intensity. At low over-potentials, the Pd- Mn_2O_3 nanocomposites show a Tafel slope of about 75 mV per decade, which is lower than the previously reported results for MnO and Mn_3O_4 supported on porous glassy carbon.²² This result indicates good electrocatalytic activity of Pd- Mn_2O_3 nanocomposites and is believed to be desirable for electrochemical applications.

Besides high activity, Pd- Mn_2O_3 nanocomposites also exhibit respectable catalytic stability in alkaline electrolyte. The catalytic durability of the 20% Pd- Mn_2O_3 nanocomposite is evaluated by applying continuous potential sweeps between -0.8 and 0.2 V in oxygen-saturated 0.1 M KOH solution for

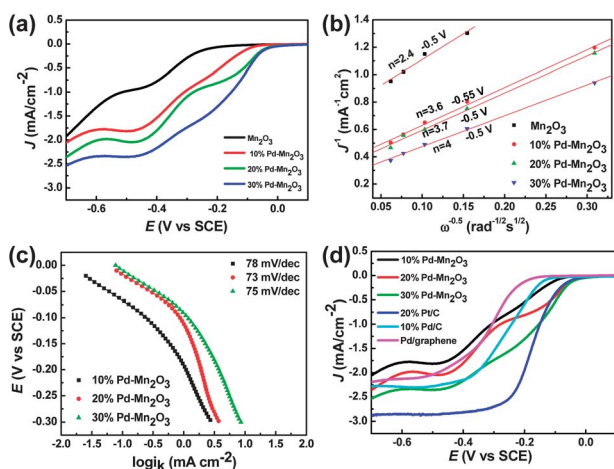


Fig. 4 (a) Linear sweep voltammograms, (b) K-L plots, (c) Tafel plots of Mn_2O_3 nanostructure and Pd- Mn_2O_3 nanocomposites and (d) linear sweep voltammograms of Pd- Mn_2O_3 nanocomposites, 20% Pt/C, 10% Pd/C and Pd/graphene in oxygen saturated 0.1 M KOH with a sweep of 10 mV s⁻¹ at 1600 rotating rates.

1000 cycles at 30 °C (Fig. 5). Upon long-term potential cycling, the ORR current density produced in the 20% Pd-Mn₂O₃ decreases by 17.4% and the onset potential has a small negative shift (Fig. 5b). As for 30% Pd-Mn₂O₃, the decline in ORR current density is only 4.8% (Fig. S9†). For commercial 20% Pt/C, 32% of the current density is lost over the cycling period, with an onset potential negative shift of 40 mV (Fig. 5d). These results demonstrate that Pd-Mn₂O₃ nanocomposites exhibited a higher catalytic stability than Pt/C in alkaline electrolyte.

Although the exact explanation requires further research, the enhancement in the catalytic activity of our obtained catalysts might be explained by the following reasons: (1) the support of Mn₂O₃ with unique mesoporous structure has higher surface area which more effectively prevents the dissociation or the migration of the tightly bound Pd nanoparticles; (2) the support itself is an attractive catalyst and shows excellent catalytic performance for ORR; (3) mesoporous Pd-Mn₂O₃ nanocomposites can permit more active sites for the contact between catalyst and electrolytes and might facilitate the diffusion, adsorption, and transport of O₂ gas; (4) loading Pd nanoparticles on the surface of mesoporous Mn₂O₃ enhances the conductivity, which should greatly favor fast electronic transfer and reduce electrode polarization during the catalytic ORR.

In summary, we have successfully synthesized a mesoporous Mn₂O₃ nanostructure. The amount of Na₃PO₄ has a great influence on the formation of the mesoporous Mn₂O₃ nanostructure. Then, Pd-Mn₂O₃ nanocomposites with different Pd loading amounts were obtained by a facile solvothermal method. Moreover, the composites of Pd-Mn₂O₃ demonstrated a good competitive ORR activity and a high selectivity, which can be comparable to the commercial Pt/C catalysts. This is attributed to the feature of mesoporous Mn₂O₃ nanostructure and the synergic effect between the Pd nanoparticles and support. To the best of our knowledge, it is the first time that mesoporous metal oxides have been used as electrocatalyst supports for ORR. Comparing the catalytic performance of different Pd loading amounts of catalysts, we found that the

catalytic activity not only depends on the loading amount of metal, but also closely relates to the porous structure of the support. The experimental results encourage us to explore and synthesize other porous metal oxide supports and metal/metal oxide nanocomposites used as electrocatalysts for ORR. The further research is on the way.

Acknowledgements

We gratefully acknowledge the financial support from the NSFC (no. 21001020, 21171096 and 21371099) and the program of Jiangsu Specially-Appointed Professor, the project funded by the Priority Academic Program Development of Jiangsu Higher Education Institutions and the Foundation of Jiangsu Collaborative Innovation Center of Biomedical Functional Materials.

Notes and references

- 1 M. K. Debe, *Nature*, 2012, **486**, 43.
- 2 R. Cao, J.-S. Lee, M. Liu and J. Cho, *Adv. Energy Mater.*, 2012, **2**, 816.
- 3 V. R. Stamenkovic, B. Fowler, B. S. Mun, G. Wang, P. N. Ross, C. A. Lucas and N. M. Markovic, *Science*, 2007, **315**, 493.
- 4 Y. Liu and C. Xu, *ChemSusChem*, 2013, **6**, 78.
- 5 A. Cao, R. Lu and G. Veser, *Phys. Chem. Chem. Phys.*, 2010, **12**, 13499.
- 6 X. Chen, G. Wu, J. Chen, X. Chen, Z. Xie and X. Wang, *J. Am. Chem. Soc.*, 2011, **133**, 3693.
- 7 S. Guo, S. Zhang, L. Wu and S. Sun, *Angew. Chem., Int. Ed.*, 2012, **51**, 11770.
- 8 J.-S. Lee, G. S. Park, H. I. Lee, S. T. Kim, R. Cao, M. Liu and J. Cho, *Nano Lett.*, 2011, **11**, 5362.
- 9 A. Dolgic, S. V. Redko, H. Bandarenka, S. L. Prischepa, K. Yanushkevich, P. Nenzi, M. Balucani and V. Bondarenko, *J. Electrochem. Soc.*, 2012, **159**, 623.
- 10 K. W. Kim, S. M. Kim, S. Choi, J. Kim and S. Lee, *ACS Nano*, 2012, **6**, 5122.
- 11 D. A. Robinson and K. J. Stevenson, *J. Mater. Chem. A*, 2013, **1**, 13443.
- 12 A. Lewera, L. Timperman, A. Roguska and N. Alonso-Vante, *J. Phys. Chem. C*, 2011, **115**, 20153.
- 13 Z. H. Zhang, X. G. Wang, Z. M. Cui, C. P. Liu, T. H. Lu and W. Xing, *J. Power Sources*, 2008, **185**, 941.
- 14 D. Xiang and L. Yin, *J. Mater. Chem.*, 2012, **22**, 9584.
- 15 J. Duan, Y. Zheng, S. Chen, Y. Tang, M. Jaroniec and S. Qiao, *Chem. Commun.*, 2013, **49**, 7705.
- 16 K. W. Kim, S. M. Kim, S. Choi, J. Kim and S. Lee, *ACS Nano*, 2012, **6**, 5122.
- 17 Y. Tan, C. Xu, G. Chen, X. Fang, N. Zheng and Q. Xie, *Adv. Funct. Mater.*, 2012, **22**, 4584.
- 18 C. H. Choi, S. H. Park and S. I. Woo, *Phys. Chem. Chem. Phys.*, 2012, **14**, 6842.
- 19 B. Lim, M. J. Jiang, P. H. C. Camargo, E. C. Cho, J. Tao, X. M. Lu, Y. M. Zhu and Y. N. Xia, *Science*, 2009, **324**, 1302.
- 20 C. Wang, H. Daimon and S. H. Sun, *Nano Lett.*, 2009, **9**, 1493.
- 21 Y. Gorlin and T. F. Jaramillo, *J. Am. Chem. Soc.*, 2010, **132**, 13612.

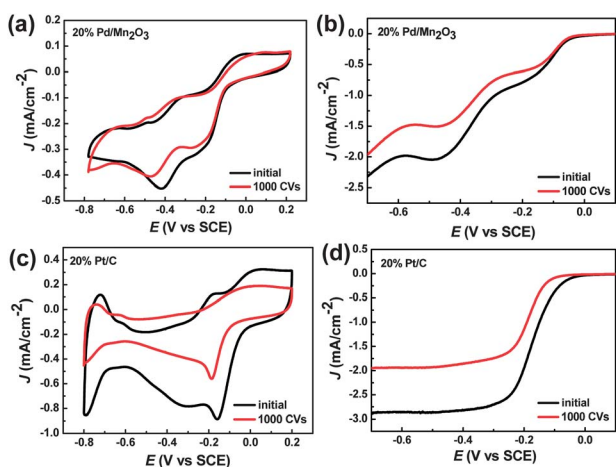


Fig. 5 CV (50 mV s⁻¹) and LSV (10 mV s⁻¹) curves for 20% Pd-Mn₂O₃ (a and b) and 20% Pt/C catalysts (c and d) before and after 1000 potential cycles in O₂-saturated 0.1 M KOH solution.

- 22 Y. Gorlis, G.-J. Chung, D. Nordlund, B. M. Clemen and T. F. Jaramillo, *ACS Catal.*, 2012, **2**, 2687.
- 23 F. Cheng, T. Zhang, Y. Zhang, J. Du, X. Han and J. Chen, *Angew. Chem., Int. Ed.*, 2013, **52**, 2474.
- 24 K. L. Pickrahn, S. W. Park, Y. Gorlin, H. Lee, T. F. Jaramillo and S. F. Bent, *Adv. Energy Mater.*, 2012, **2**, 1269.
- 25 F. Cheng, J. Shen, B. Peng, Y. Pan, Z. Tao and J. Chen, *Nat. Mater.*, 2011, **10**, 780.
- 26 M. Chigane and M. Ishikawa, *J. Electrochem. Soc.*, 2000, **147**, 2246.
- 27 J. F. Moulder, W. F. Stickle, P. E. Sobol and K. D. Bomben, *Handbook of X-Ray Photoelectron Spectroscopy*, Physical Electronics, Inc., Eden Prairie, MN, 1995, p. 119.